A Novel 3D Space-Time-Frequency Non-Stationary Channel Model for 6G THz Indoor Communication Systems

Jun Wang[1,3], Cheng-Xiang Wang[1,3,*], Jie Huang[1,3], Haiming Wang[2,3]

[1]National Mobile Communications Research Laboratory, School of Information of Science and Engineering, Southeast University, Nanjing 210096, China.

[3]State Key Laboratory of Millimeter Waves, School of Information of Science and Engineering, Southeast University, Nanjing 210096, China.

[2]Purple Mountain Laboratories, Nanjing 211111, China.

[*]Corresponding Author: Cheng-Xiang Wang

Email: {jun.wang, chxwang, j_huang, hmwang}@seu.edu.cn

Abstract—**Terahertz (THz) communication is now being considered as one of possible technologies for the sixth generation (6G) communication systems. In this paper, a novel three-dimensional (3D) space-time-frequency non-stationary massive multiple-input multiple-output (MIMO) channel model for 6G THz indoor communication systems is proposed. In this geometry-based stochastic model (GBSM), the initialization and evolution of parameters in time, space, and frequency domains are developed to generate the complete channel transfer function (CTF). Based on the proposed model, the correlation functions including time auto-correlation function (ACF), spatial cross-correlation function (CCF), and frequency correlation function (FCF) are investigated. The results show that the statistical properties of the simulation model match well with those of the theoretical model. The stationary intervals at different frequencies are simulated. The non-stationarity in time, space, and frequency domains is verified by theoretical derivations and simulations.**

Index Terms—**THz channel model, massive MIMO, GBSM, space-time-frequency non-stationarity**

I. INTRODUCTION

With the rapid development of wireless communication, the data traffic is expected to grown exponentially in the 6G communication system. THz communication is considered as one of the most important key technologies for 6G communication systems. THz wave from 0.1 THz to 10 THz have the ability to provide large bandwidth of more than one hundred gigahertz(GHz) [1]. As a result, THz communication can theoretically achieve ultra-high transmission rate of 100 Gbps or even higher [2].

For the design and optimization of THz communication systems, a THz channel model that can accurately reflect THz characteristics is necessary. An accurate channel model is also the prerequisite for performance evaluation of the communication systems such as capacity analysis [3] and energy efficiency evaluation [4]. Traditional channel models for lower frequency can not be applied to THz band due to some unique characteristics in THz band such as path loss and propagation properties. Path loss and atmospheric absorption of THz channels were investigated in [5]–[7]. The gas absorption caused by oxygen and water vapor will rapidly increase when the frequency becomes higher.

Propagation properties of THz waves were studied in the literature. In [8], [9], measurement and modeling of multiple reflection effects in building materials at THz were introduced. The reflection loss shows great dependence on frequency and materials and can be calculated by Kirchhoff theory. According to the measurement in [10], high-order paths are very hard to be detected due to high reflection loss. The diffusely scattered propagation was investigated in [11]–[14]. In THz band, more power is diffusely scattered when frequency increases. All the diffusely scattered rays happen around the specular reflected path and scattering remote from the immediate region around the specular reflection points can be neglected during the channel modeling. However, most of the measurements of channel characteristics were carried out at 300 GHz, channel characteristics of reflection and scattering in higher frequencies need to be investigated experimentally.

Many THz channel models were proposed for indoor THz communications. In [15], a novel channel model based on ray tracing was proposed, which incorporated the propagation models for the line-of-sight (LOS), reflected, scattered, and diffracted paths. This channel model was validated with the experimental measurements from the literature. In [16], a stochastic channel model for indoor scenarios considering frequency dispersion was proposed. However, channel models based on ray tracing methods are not general and flexible. The existing stochastic THz channel models cannot show the unique propagation characteristics of THz waves in the indoor scenario and they do not support dynamic environments. In addition, some non-stationary channel models for millimeter wave band communication systems were proposed in [17]–[20]. However, the evolution of clusters in these channel models are not suitable for THz band channel models.

In this paper, a 3D space-time-frequency non-stationary GBSM for THz communication systems is proposed. The
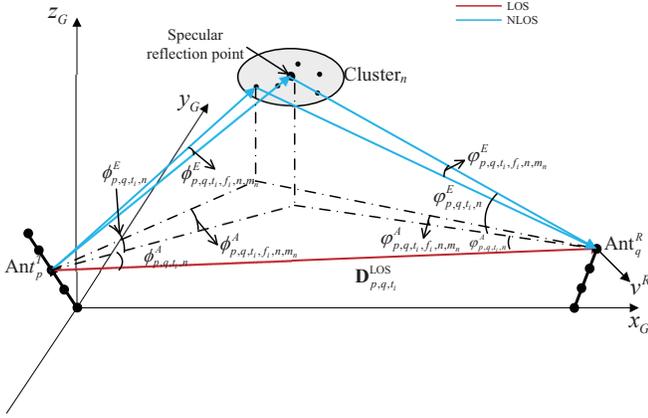
Fig. 1. A 3D THz GBSM for indoor communication.

mobility of users and ultra massive MIMO are considered for THz indoor communication systems to model the non-stationarity in time and space domains. In frequency domain, we consider that diffusely scattering in a surface is frequency dependent according to the investigation of THz propagation. To obtain the space-time-frequency dependent channel coefficient, we will first initialize the channel at first element of transmitter (Tx) and receiver (Rx), time t_0, and frequency f_0. Then the channel evolution will be taken in time, space, and frequency domains. After the space-time-frequency dependent CTF is generated, channel characteristics such as delay power spectrum density (PSD), ACF , CCF and FCF are studied.

The remainder of this paper is organized as follows. Section II describes the proposed GBSM in details and gives the CTF of the channel. In Section III, channel characteristics are calculated. Then simulation results are compared and analyzed in Section IV. Finally, conclusions are drawn in Section V.

II. A NOVEL 3D THZ MIMO GBSM

A. Description of the Channel Model

Let us consider a MIMO indoor communication system equipped with M_T transmit and M_R receive antennas. The center frequency is f_c. Let Ant_p^T denote the pth transmitted antenna and Ant_q^R denote the qth received antenna. It should be noted that arbitrary antenna array layouts can be considered in the proposed model.

The proposed non-stationary THz GBSM is illustrated in Fig. 1. In THz band, the wavelength of the carrier frequency is less than one millimeter and comparable to the roughness of some common materials. In this model, each cluster is comprised of diffuse sacttering rays from one roughness surfaces. The center of cluster is considered as specular reflected point. Notice that coordinate (x_G, y_G, z_G) is established as the global coordinate system (GCS) whose origin is at the first element of the transmit antenna array. This needs to be distinguished from the local coordinate system (LCS) whose origins are at the centers of transmit and receive antenna arrays when calculating 3D radiation pattern.

Let $\mathbf{A}_{p,t_i}^T$ and $\mathbf{A}_{q,t_i}^R$ denote the position vectors of Ant_p^T and Ant_q^R at time t_i, respectively. Also, let ψ_A^T and ψ_E^T be azimuth and elevation angles of the transmit array, and let ψ_A^R and ψ_E^R be azimuth and elevation angles of the receive array, respectively. $\mathbf{D}$ represents the initial position vector of the receiver and it is assumed to be $[D_0, 0, 0]^T$. D_0 is the initial distance between the first elements of Tx and Rx at time t_0.

The LOS distance vector $\mathbf{D}_{p,q,t_i}^{\text{LOS}}$ is computed as

$$\mathbf{D}_{p,q,t_i}^{\text{LOS}} = \mathbf{D} + \mathbf{A}_{q,t_i}^R - \mathbf{A}_{p,t_i}^T + \mathbf{v}^R(t_n - t_0). \qquad (1)$$

It is clear that $\mathbf{D}$ equals $\mathbf{D}_{1,1,t_0}^{\text{LOS}}$. Also, the distance between Ant_p^T and Ant_q^R at time t_i is $D_{p,q,t_i}^{\text{LOS}} = \|\mathbf{D}_{p,q,t_i}^{\text{LOS}}\|$, where $\|\cdot\|$ calculates the Frobenius norm.

B. The Theoretical Model

In this channel model, the LOS and non-LOS (NLOS) components are considered. The NLOS components are combined of single bounce and double bounce paths. Higher order paths are neglected due to very high reflection loss.

Considering the space-time-frequency non-stationarity, the CTF at time t_i and frequency f_i can be characterized by an $M_T \times M_R$ matrix $\mathbf{H}_{t_i,f_i}(f) = [H_{p,q,t_i,f_i}(f)]_{M_T \times M_R}$. The element of the matrix means the CTF for pth transmit element and qth receive element, and can be expressed as

$$
H_{p,q,t_i,f_i}(f) = H_{p,q,t_i}^{\text{LOS}}(f) \\
+ \sum_{n=1}^{N} \sum_{m_n=1}^{M_n} \lim_{M_n \to \infty} H_{p,q,t_i,f_i,n,m_n}^{\text{NLOS}}(f) \qquad (2)
$$

where N is number of clusters including single bounce and double bounce clusters, M_n is the number of rays within Cluster$_n$. In this model, N is generated randomly, but it is a constant during the generation of channel coefficients. The subscript t_i and f_i mean specific time and frequency.

1) LOS: For the LOS component, if polarized antenna arrays are assumed at both the Tx and Rx sides, the complex channel coefficient $H_{p,q,t_i}^{\text{LOS}}(f)$ is presented as

$$
H_{p,q,t_i}^{\text{LOS}}(f) = \\
\begin{bmatrix} F_{p,V}^T(\phi_{E,p,q,t_i}^{\text{LOS}}, \phi_{A,p,q,t_i}^{\text{LOS}}, f_i) \\ F_{p,H}^T(\phi_{E,p,q,t_i}^{\text{LOS}}, \phi_{A,p,q,t_i}^{\text{LOS}}, f_i) \end{bmatrix}^T \begin{bmatrix} e^{j\Phi_{\text{LOS}}} & 0 \\ 0 & -e^{j\Phi_{\text{LOS}}} \end{bmatrix} \\
\begin{bmatrix} F_{p,V}^T(\varphi_{E,p,q,t_i}^{\text{LOS}}, \varphi_{A,p,q,t_i}^{\text{LOS}}, f_i) \\ F_{p,H}^T(\varphi_{E,p,q,t_i}^{\text{LOS}}, \varphi_{A,p,q,t_i}^{\text{LOS}}, f_i) \end{bmatrix} \sqrt{P_{p,q,t_i,f_i}^{\text{LOS}}} e^{-j2\pi f \tau_{p,q,t_i}^{\text{LOS}}} \qquad (3)
$$

where Φ_{LOS} is uniformly distributed within $(0, 2\pi)$. The superscripts V and H denote vertical polarization and horizontal polarization, respectively. Functions $F^T(a,b,f)$ and $F^R(a,b,f)$ are frequency dependent antenna patterns with input angles a and b in the GCS. The input angles a and b need to be transformed into the LCS to obtain the antenna patterns. $\tau_{p,q,t_i}^{\text{LOS}}$ is the delay from Ant_{p,t_i}^T to Ant_{q,t_i}^R at time t_i which is decided by the distance $\tau_{p,q,t_i}^{\text{LOS}} = D_{p,q,t_i}^{\text{LOS}}/c$.

TABLE I
DEFINITION OF MAIN PARAMETERS.

Parameters	Definition
$\mathbf{D}$	Initial 3D distance between the T_x and the R_x at t_0
$\mathbf{A}_{p,t_i}^T$, $\mathbf{A}_{q,t_i}^R$	3D vector from the first element of transmit array/receive array at t_0 to Ant_p^T, Ant_q^R at t_i
$\mathbf{v}^T$, $\mathbf{v}^R$	3D velocity vector of transmit and receive array
$\mathbf{D}_{p,q,t_i}^{LOS}$	3D distance vector of the LOS component between Ant_p^T and Ant_q^R at t_i
D_{p,q,t_i}^{LOS}	Distance vector of the LOS component between Ant_p^T and Ant_q^R at t_i
$\phi_{p,q,t_i}^{A,LOS}$, $\phi_{p,q,t_i}^{E,LOS}$	Azimuth and elevation angles of departure between Ant_p^T and Ant_q^R at t_i
$\varphi_{p,q,t_i}^{A,LOS}$, $\varphi_{p,q,t_i}^{E,LOS}$	Azimuth and elevation angles of arrival between Ant_p^T and Ant_q^R at t_i
N	Total number of observable NLOS clusters
M_n	Numbers of rays within Cluster_n
$\tilde{A}_{p,q,t_i,n}$	Mirror position of Ant_{p,t_i}^T for Cluster_n at t_i
$\tilde{\mathbf{D}}_{p,q,t_i,n}$	3D vector from $\tilde{A}_{p,q,t_i,n}$ to Ant_q^R for Cluster_n at t_i
$P_{p,q,t_i,f_i,n}$	Mean power of the nth cluster between Ant_p^T and Ant_q^R at t_i and f_i
$\tau_{p,q,t_i,n}$	Delay from Ant_p^T to Ant_q^R via Cluster_n at t_i
τ_{p,q,t_i,f_i,n,m_n}	Relative delay from Ant_p^T to Ant_q^R via mth ray in Cluster_n at t_i and f_i
$\phi(\varphi)_{p,q,t_i,n}^A, \phi(\varphi)_{p,q,t_i,n}^E$	Azimuth and elevation angles of departure(arrival) between Cluster_n and Ant_p^T at t_i
$\phi(\varphi)_{p,q,t_i,n,m_n}^A, \phi(\varphi)_{p,q,t_i,n,m_n}^E$	Azimuth and elevation angles of departure(arrival) between m_nth ray of Cluster_n and Ant_p^T at t_i and f_i

To make the proposed channel model more realistic, the path loss composes of free space path loss and the atmosphere absorption. Here, the atmosphere absorption is a function of distance, wavelength, and some environment parameters such as temperature and humidity. To simplify the channel model, we assume the atmosphere absorption is only decided by distance and wavelength. The path loss in dB is given by

$$P_{f_i}^{\text{LOS}}(D)[\text{dB}] = 20 log_{10}(\frac{4\pi D}{\lambda_i}) + L_a(D, \lambda_i) + X(\sigma). \quad (4)$$

Here, λ_i is the wavelength of frequency f_i, $20 log_{10}(\frac{4\pi D}{\lambda_i})$ is free space path loss, $L_a(D, \lambda_i)$ is the atmosphere absorption, and $X(\sigma)$ is the random loss caused by the system. In this model, P_{p,q,t_i,f_i}^{LOS} can be expressed as $P_{p,q,t_i,f_i}^{\text{LOS}} = P_{f_i}^{\text{LOS}}(D_{p,q,t_i}^{\text{LOS}})$. The angle of departure (AoD) is equal to angle of arrival (AoA) for the LOS path. The azimuth/elevation angle of departure (AAoD/EAoD) $\phi_{A,p,q,t_i}^{\text{LOS}}/\phi_{E,p,q,t_i}^{\text{LOS}}$ and azimuth/elevation angle of arrival (AAoA/EAoA) $\varphi_{A,p,q,t_i}^{\text{LOS}}/\varphi_{E,p,q,t_i}^{\text{LOS}}$ can be calculated by the vector $\mathbf{D}_{p,q,t_i}^{\text{LOS}}$.

2) NLOS: The CTF of the m_nth ray in cluster_n is

$$H_{p,q,t_i,f_i,n,m_n}(f) =$$
$$\begin{bmatrix} F_{p,V}^T(\tilde{\phi}_{p,q,t_i,f_i,n,m_n}^E, \tilde{\phi}_{p,q,t_i,f_i,n,m_n}^A, f_i) \\ F_{p,H}^T(\tilde{\phi}_{p,q,t_i,f_i,n,m_n}^E, \tilde{\phi}_{p,q,t_i,f_i,n,m_n}^A, f_i) \end{bmatrix}^T$$
$$\begin{bmatrix} \sqrt{k_{n,m_n}^{-1}}e^{j\Phi_{n,m_n}^{VV}} & e^{j\Phi_{n,m_n}^{VH}} \\ e^{j\Phi_{n,m_n}^{HV}} & \sqrt{k_{n,m_n}^{-1}}e^{j\Phi_{n,m_n}^{HH}} \end{bmatrix}$$
$$\begin{bmatrix} F_{p,V}^T(\tilde{\varphi}_{p,q,t_i,f_i,n,m_n}^E, \tilde{\varphi}_{p,q,t_i,f_i,n,m_n}^A, f_i, f_i) \\ F_{p,H}^T(\tilde{\varphi}_{p,q,t_i,f_i,n,m_n}^E, \tilde{\varphi}_{p,q,t_i,f_i,n,m_n}^A, f_i, f_i) \end{bmatrix}$$
$$\sqrt{\frac{P_{p,q,t_i,f_i,n}}{M_n}}e^{-j2\pi f(\tau_{p,q,t_i,n} + \tau_{p,q,t_i,f_i,n,m_n})}. \quad (5)$$

In (5), $P_{p,q,t_i,f_i,n}$ is the power of Cluster_n, $\tau_{p,q,t_i,n}$ and τ_{p,q,t_i,f_i,n,m_n} are delay of cluster_n and relative delay of m_nth ray in Cluster_n, respectively, k_{n,m_n} denotes the cross polarization power ratio, Φ_{n,m_n}^{VV}, Φ_{n,m_n}^{VH}, Φ_{n,m_n}^{HV}, and Φ_{n,m_n}^{HH} are the initial random phases of the m_nth ray in $Cluster_n$ in four polarization directions. Parameters $\tilde{\phi}_{p,q,t_i,f_i,n,m_n}^E$, $\tilde{\phi}_{p,q,t_i,f_i,n,m_n}^A$, $\tilde{\varphi}_{p,q,t_i,f_i,n,m_n}^E$, and $\tilde{\varphi}_{p,q,t_i,f_i,n,m_n}^A$ are EAoD, AAoD, EAoA, and AAoA, respectively. It should be noted that $\tilde{\phi}$ means the summation of angle of a cluster and the relative angle. For example,

$$\tilde{\phi}_{p,q,t_i,f_i,n,m_n}^E = \phi_{p,q,t_i,n}^E + \phi_{p,q,t_i,f_i,n,m_n}^E. \quad (6)$$

Similarly, $\tilde{\phi}_{p,q,t_i,f_i,n,m_n}^A$, $\tilde{\varphi}_{p,q,t_i,f_i,n,m_n}^E$, and $\tilde{\varphi}_{p,q,t_i,f_i,n,m_n}^A$ can be calculated similarly. The definitions of main parameters are given in Table I.

C. The Simulation Model

In the simulation model, the number of rays within a cluster is assumed as infinite in this theoretical model while it is finite in the simulation model which can be expressed as

$$H_{p,q,t_i,f_i}(f) = H_{p,q,t_i}^{\text{LOS}}(f) + \sum_{n=1}^{N}\sum_{m_n=1}^{M_n} H_{p,q,t_i,f_i,n,m_n}^{\text{NLOS}}(f). \quad (7)$$

In the simulation model, the method of equal area (MEA) [21] is used to obtain the discrete AAoDs, EAoDs, AAoAs, and EAoAs.

D. Channel Initialization

In this subsection, channel initialization is discussed. All the parameters for NLOS components are generated for p=1, q=1 at time t_0 and frequency f_0. After these parameters are generated, evolution of them will be taken which is introduced in the next subsection.

The number of paths is generated randomly for first bounce and second bounce paths, respectively. For first order path, the number N_{1st} has the probabilities of $p(4) = 0.35$ and $p(5) = 0.65$. For second order reflection, the number N_{2nd} ranges from 7 to 13. The total number of paths is constant during the evolution. It is clear that $N = N_{1st} + N_{2nd}$.

The initial cluster delay $\tau_{1,1,t_0,n}$ is generated by random variables $\Delta\tau_{i,1st}$ and $\Delta\tau_{i,2nd}$ [16], where $\Delta\tau_{i,1st}$ and $\Delta\tau_{i,2nd}$ is defined as the time interval of arrival between two adjacent clusters for first order cluster and second order cluster, respectively. For first cluster, $\Delta\tau_1$ is the time interval compared to the LOS path. So, we have

$$\tau_{1,1,t_0,i} = \begin{cases} \tau_{1,1,t_0}^{LOS} + \Delta\tau_{i,1st}, & i = 1; \\ \tau_{1,1,t_0,i-1} + \Delta\tau_{i,1st}, & 2 \leq i \leq N_{1st}. \end{cases} \quad (8)$$

A similar method is used to generate second bounce clusters which can be expressed as

$$\tau_{1,1,t_0,i} = \begin{cases} \tau_{1,1,t_0}^{LOS} + \Delta\tau_{i,2nd}, & i = N_{1st} + 1; \\ \tau_{1,1,t_0,i-1} + \Delta\tau_{i,2nd}, & N_{1st} + 2 \leq i \leq N \end{cases} \quad (9)$$

where $\Delta\tau_{i,1st}$ and $\Delta\tau_{i,2nd}$ are negative exponential (NEXP) random variables with parameters $\mu_{\Delta\tau_{i,1st}}$ and $\mu_{\Delta\tau_{i,2nd}}$. The relative delay $\tau_{1,1,t_0,f_0,n,m_n}$ is also considered as a NEXP random variable with the parameter $\mu_{f_i,n}$.

The power of the cluster is generated according to the distance [16]. It can be expressed as

$$P_{1,1,t_0,i}(dB) = P_{1,1,t_0}^{LOS} - \Delta P_{1,1,t_0}^{LOS} - n_\tau \cdot (\tau_{1,1,t_0,i} - \tau_{1,1,t_0}^{LOS}) + \Delta a_i \quad (10)$$

where $P_{1,1,t_0}^{LOS}$ is the function value at the LOS delay with respect to the LOS amplitude, and n_τ is the temporal decay coefficient. Moreover, each ray deviates from the straight line by the random variable Δa_i.

The initial phase of each cluster is considered as uniformly distributed in $[-\pi, \pi]$. The EAoD, AAoD, EAoA, and AAoA of the initial position and time are considered as independent Gaussian distributions. The relative angles $\phi_{1,1,t_0,f_0,n,m_n}^E$, $\phi_{1,1,t_0,f_0,n,m_n}^A$, $\varphi_{1,1,t_0,f_0,n,m_n}^E$, and $\varphi_{1,1,t_0,f_0,n,m_n}^A$ are Gaussian distributed with zero mean and independent variance $\sigma_{f_i,n}$.

E. Evolution of Clusters

In this subsection, the space, time, and frequency domain cluster evolutions for the proposed THz channel model are demonstrated. The flow chart is shown in Fig. 2. Here, we update the parameters for each cluster in time and space domains based on the geometric relationship. Evolution in frequency domain is also considered as the regeneration of relative distance and relative angle in different frequency points.

1) Evolution in the Time Domain: The Rx is assumed to move to imitate human activity in an indoor office. Usually, the velocity of Rx is small. In a small time interval, the difference of positions is small. We assume that the specular reflection point is still on the same surface, but the position is moving a
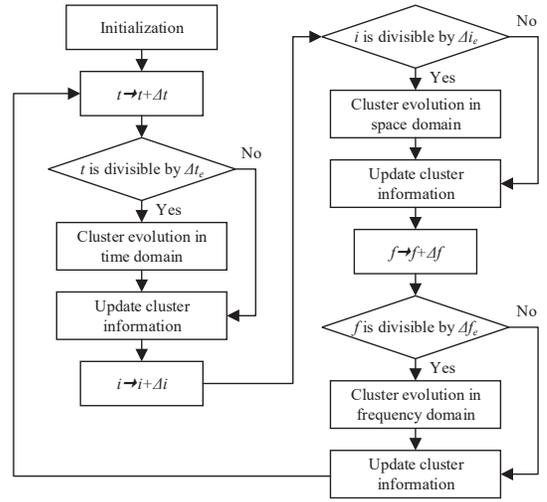

Fig. 2. The flowchart of space-time-frequency cluster evolution of the proposed THz channel model.

small distance. Here, we use a single reflection as an example and the geometric relationship is shown in Fig. 3.

Let us use $\tilde{A}_p^T$ to denote the mirror point of Tx point reflection and $\mathbf{D}_{t+\Delta t,p,q,f,n}$ represent the virtual vector from $\tilde{A}_p^T$ to Ant_{q,t_i}^R. This virtual point keeps static when the Rx is moving. For the initial time and position, we have

$$\mathbf{D}_{1,1,t_0 n} = \begin{bmatrix} D_{1,1,t_0,n} \cos\varphi_{p,q,t_0,n}^E \cos\varphi_{p,q,t_0,n}^A \\ D_{1,1,t_0,n} \cos\varphi_{p,q,t_0,n}^E \sin\varphi_{p,q,t_0,n}^A \\ D_{1,1,t_0,n} \sin\varphi_{p,q,t_0,n}^E \end{bmatrix}. \quad (11)$$

The new distance $D_{t+\Delta t,p,q,f,n}$ at $t + \Delta t$ of $Cluster_n$ can be calculated by

$$\begin{aligned} D_{t+\Delta t,p,q,f,n} &= \left\| \tilde{\mathbf{D}}_{p,q,t_i+\Delta t,n} \right\| \\ &= \left\| \tilde{\mathbf{D}}_{p,q,t_i,n} + \mathbf{v}^R \Delta t \right\|. \end{aligned} \quad (12)$$

The EAoA and AAoA at $t_i + \Delta t$ $\phi_{p,t,n}^E$ and $\phi_{p,t,n}^A$ equal to elevation and azimuth angle of the virtual vector $\mathbf{D}_{p,q,t_i+\Delta t,n}$, respectively. Then, the EAoD and AAoD can be calculated as

$$\phi_{p,q,t_i+\Delta t,n}^E = \phi_{p,q,t_i,n}^E + \varphi_{p,q,t_i+\Delta t,n}^E - \varphi_{p,q,t_i,n}^E \quad (13)$$

$$\phi_{p,q,t_i+\Delta t,n}^A = \phi_{p,q,t_i,n}^A + \varphi_{p,q,t_i+\Delta t,n}^A - \varphi_{p,q,t_i,n}^A. \quad (14)$$

The power of the cluster is also re-calculated according to the updated distance at $t + \Delta t$. Similarly, the phase of the cluster is also updated according to the updated distance. However, the relative delay and relative angle dispersion is considered invariant during time evolution.

2) Evolution in the Space Domain: The process of evolution in the space domain is similar to the algorithm in the time domain. Evolution in the space domain is also calculated by geometric relationship. The 3D distance between adjacent elements replaces the mobility in the time domain.
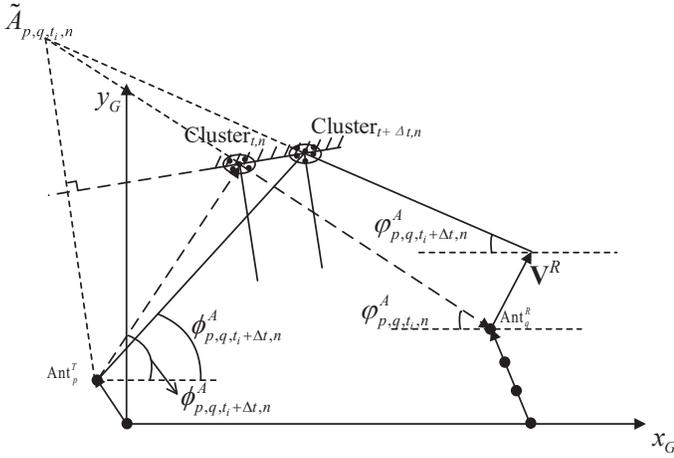
Fig. 3. Illustration of evolution in the time domain.

3) Evolution in the Frequency Domain: The scattering from one surface does not keep the same at different frequencies because of different wavelengths. All the intra-cluster parameters including relative delay and relative angle need to be updated when frequency changes. Relative delay is re-generated with new $\mu_{f_i,n}$ by

$$\mu_{f_i,n} = \mu_{f_0,n} \times (\frac{f_i}{f})^{\rho_\mu}. \tag{15}$$

Similarly, relative angles need to be generated with the $\sigma_{f_i,n}$ by

$$\sigma_{f_i,n} = \sigma_{f_0,n} \times (\frac{f_i}{f})^{\rho_\sigma}. \tag{16}$$

Then, the channel coefficient at frequency f_i can be generated.

III. STATISTICAL PROPERTIES

In this section, some typical statistical properties of the proposed non-stationary theoretical THz channel model are derived.

A. The Delay PSD

The delay PSD $\Upsilon_{p,q,t_i,f_i}(\tau)$ can be written as

$$\Upsilon_{p,q,t_i,f_i}(\tau) = \left|h_{p,q,t_i}^{\text{LOS}}\right|^2 \times \delta(\tau - \tau_{p,q,t_i}^{\text{LOS}})$$
$$+ \sum_{n=1}^{N} \sum_{m_n=1}^{M_n} \left|h_{p,q,t_i,f_i,n,m_n}\right|^2 \tag{17}$$
$$\times \delta(\tau - \tau_{p,q,t_i,n} - \tau_{p,q,t_i,f_i,n,m_n}).$$

This cluster power at different delays can be calculated from the channel impulse response (CIR) $h_{p,q,t_i,f_i,n,m_n}\delta(\tau - \tau_{p,q,t_i,n} - \tau_{p,q,t_i,f_i,n,m_n})$, which is the inverse Fourier transform of CTF.

B. Space-Time-Frequency Correlation Function

The space-time-frequency correlation function $R_{p,q,t_i,q_i}(\Delta p, \Delta q, \Delta t, \Delta f)$ can be calculated as

$$R_{p,q,t_i,f_i}(\Delta p, \Delta q, \Delta t, \Delta f)$$
$$= E\left[H_{p,q,t_i,f_i}(f) \cdot H^*_{p+\Delta q, q+\Delta p, t_i+\Delta t, f_i+\Delta f}(f)\right]$$
$$= \frac{K}{K+1} R_{p,q,t_i,f_i}^{\text{LOS}}(\Delta p, \Delta q, \Delta t, \Delta f) \tag{18}$$
$$+ \frac{1}{K+1} R_{p,q,t_i,f_i}^{\text{NLOS}}(\Delta p, \Delta q, \Delta t, \Delta f)$$

where $E[\cdot]$ denotes the expectation operator, $(\cdot)^*$ denotes the complex conjugate operation, K is the Ricean factor which is the ratio of the LOS power to the NLOS power and it can be calculated from the CTF. The correlation function of the channel consists of the LOS and NLOS components.

–In the LOS case,

$$R_{p,q,t_i,f_i}^{\text{LOS}}(\Delta p, \Delta q, \Delta t, \Delta f)$$
$$= E\left[H_{p,q,t_i,f_i}^{\text{LOS}}(f) \cdot H_{p+\Delta q, q+\Delta p, t_i+\Delta t, f_i+\Delta f}^{\text{LOS}*}(f)\right]. \tag{19}$$

–In the NLOS case,

$$R_{p,q,t_i,q_i}^{\text{NLOS}}(\Delta p, \Delta q, \Delta t, \Delta f)$$
$$= E\left[\sum_{n=1}^{N} \sum_{m_n=1}^{M_n} H_{p,q,t_i,f_i,n,m_n}(f)\right. \tag{20}$$
$$\left. \times H^*_{p+\Delta q, q+\Delta p, t_i+\Delta t, f_i+\Delta f, n, m_n}(f)\right].$$

By setting partial parameters of $(\Delta p, \Delta q, \Delta t, \Delta f)$ as 0, the space-time-frequency correlation function can easily be simplified to FCF, time ACF and spatial CCF, which can be expressed as

$$R_{p,q,t_i,f_i}^{\text{FCF}}(\Delta f) = R_{p,q,t_i,f_i}(0,0,0,\Delta f) \tag{21}$$
$$R_{p,q,t_i,f_i}^{\text{ACF}}(\Delta t) = R_{p,q,t_i,f_i}(0,0,\Delta t,0) \tag{22}$$
$$R_{p,q,t_i,f_i}^{\text{CCF}}(\Delta p, \Delta q) = R_{p,q,t_i,f_i}(\Delta p, \Delta q, 0, 0). \tag{23}$$

C. The Stationary Intervals in Space-Time-Frequency Domain

The stationary interval is the period during which the channel statistical properties can be seen as unchanged. To obtain the stationary interval in space-time-frequency domain, the time-variant correlation matrix distance (CMD) can be applied [22]. The CMD can be calculated in space-time-frequency domain as follows

$$d_{\text{corr}}(\Delta p_s, \Delta q_s, \Delta t_s, \Delta f_s)$$
$$= \frac{tr\{R_{p,q,t_i,f_i} R_{p+\Delta p_s, q+\Delta q_s, t_i+\Delta t_s, f_i+\Delta f_s}\}}{\|R_{p,q,t_i,f_i}\| \|R_{p+\Delta p_s, q+\Delta q_s, t_i+\Delta t_s, f_i+\Delta f_s}\|} \tag{24}$$

where R_{p,q,t_i,f_i} is the correlation function of channel transfer function. The stationary interval can expressed as

$$RG(p,q,t_i,f_i) =$$
$$\min\{\Delta p_s, \Delta q_s, \Delta t_s, \Delta f_s \mid_{d_{\text{corr}}(\Delta p_s, \Delta q_s, \Delta t_s, \Delta f_s) \geqslant c_{th}}\} \tag{25}$$

where Δp_s and Δq_s are the space stationary interval at Tx and Rx,respectively. Δt_s is the time stationary interval, and
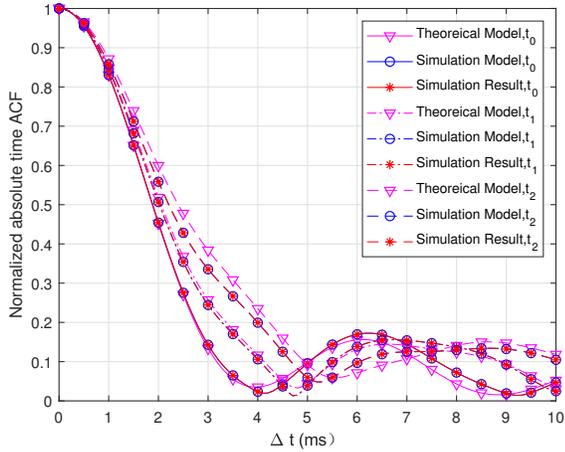
Fig. 4. The comparison of time-variant ACF of theoretical model, simulation model, and simulation results at t_0=0 s, t_1=5 s, and t_2=10 s (p=1, q=1, f_i=300 GHz, v^R=0.1 m/s).
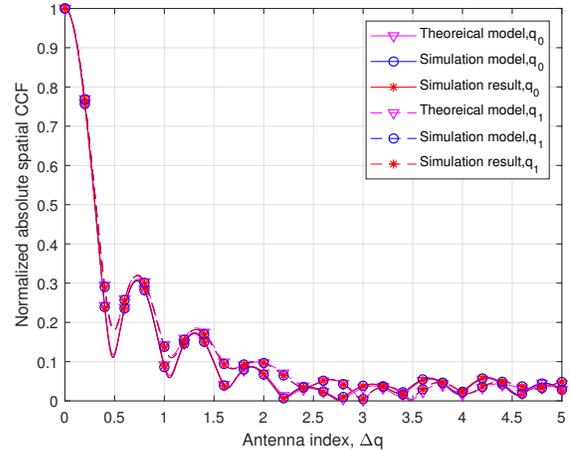

Fig. 5. The comparison of spatial CCFs of theoretical model, simulation model, and simulation results at q_0=1,q_1=1000 (p=1, t_0=0s, f_i=300 GHz, v^R=0.1 m/s).

Δf_s is the frequency stationary. c_{th} is the threshold which can be adjusted in different cases. The above stationary intervals can be used to evaluate the non-stationary behaviors of THz channels in space/time/frequency domains.

IV. RESULTS AND DISCUSSIONS

In this part, the statistical properties of the proposed THz channel models are studied and analyzed. The antenna arrays of Tx and Rx are assumed to be uniform linear array (ULA). The element of the array is assumed as omnidirectional and the gain is 1 in all directions. The related parameters are listed as follows. The moving speed of Rx is v^R = 0.1 m/s with the direction angle $\theta^E = 0$ and $\theta^A = \frac{\pi}{3}$ while the Tx is fixed. The frequency band is chosen from 300 GHz to 400 GHz. The numbers of antenna elements at the Tx and Rx were both set as 1024. The initial distance between the first elements of Tx and Rx is 3 m, $\mu_{\Delta\tau_{i,1st}}$ and $\mu_{\Delta\tau_{i,2nd}}$ are set as 2.73 ns and 4.8 ns, respectively. All the initial angle parameters are generated by Gaussian distribution. The standard deviations of $\phi^A_{1,1,t_0,n}$, $\phi^E_{1,1,t_0,n}$,$\varphi^A_{1,1,t_0,n}$, and $\varphi^E_{1,1,t_0,n}$ are set as 1.2. The ρ_μ and ρ_σ are set as 3. The number of rays in each cluster is set as 100.

A. ACF

By setting $\Delta p, \Delta q, \Delta f$ as 0, the time ACF of the theoretical model can be obtained. The comparison of theoretical model, simulation model, and simulation result at t_0=0 s, t_1=5 s, and t_2=10 s of Cluster$_1$ is shown in Fig. 4. From the results, we can see that the simulation model provides a good approximation to the theoretical model. We can observe different time ACFs at different time instants, which demonstrates that the proposed model can capture the non-stationarity of channel in the time domain.

B. Spatial CCF

The comparison of the theoretical model, simulation model, and simulation result for Cluster$_1$ with different receive elements is shown in Fig. 5. we can see that the differences of
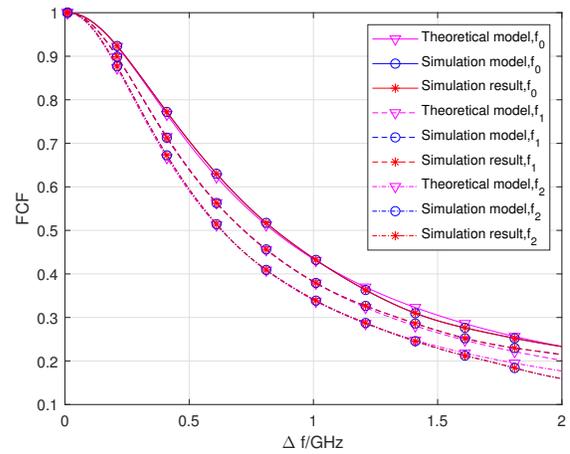

Fig. 6. The comparison of FCFs of theoretical model, simulation model, and simulation results at f_0=300 GHz, f_1=325 GHz, and f_2=350 GHz (p=1, q=1, t_0=0 s, v^R=0.1 m/s).

two spatial CCFs are quite similar because the antenna spacing is not large because the antenna spacing is quite small in THz band. However, the differences are still observable. If the antenna size is large enough, non-stationarity of THz channel in the space domain should be considered.

C. FCF

The results of FCF at different f_0=300 GHz, f_1=325 GHz, and f_2 = 350 GHz are shown in Fig. 6. We can observe the differences of FCF at different frequencies are small clearly in the picture. Due to the frequency dependent intra-cluster parameters, the channel can not be considered as stationary in frequency domain.

D. Stationary Interval

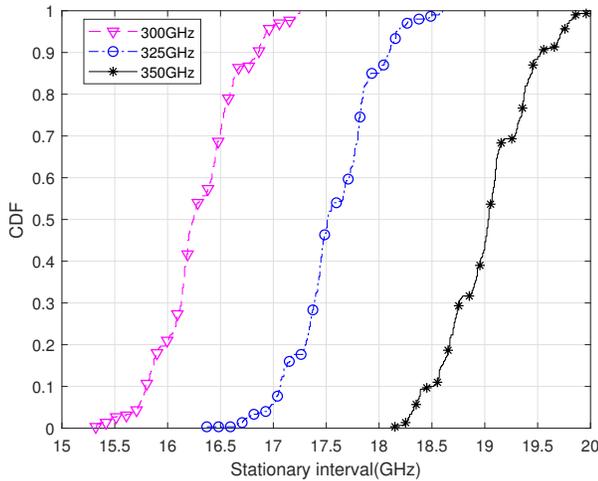The stationary intervals of the simulation model are obtained by 5000 times of Monte Carlo simulations. The CCDFs

Fig. 7. The comparison of stationary interval of the simulation model in frequency domain at f_0=300 GHz, f_1=325 GHz and f_2=350 GHz (p=1, q=1, t_0=0 s, v^R=0.1 m/s), $c_{th} = 0.9$.

of the stationary intervals in frequency domain of the proposed channel model in different frequencies are shown in Fig. 7. The threshold is set as 0.9. The channel whose bandwidth less than the stationary interval can be considered as frequency stationary. For higher frequency, the frequency stationary interval will linearly increase.

V. CONCLUSIONS

In this paper, a novel 3D space-time-frequency non-stationary THz massive MIMO channel model for 6G THz indoor communication systems has been proposed. The initialization and evolution of parameters in time, space, and frequency domains have been given to generate the complete channel. Based on the proposed models, the correlation functions including ACF, CCF, and FCF have been investigated. Numerical and simulation results have shown that the statistical properties of the simulation model match well with those of the theoretical model. The non-stationarity in time, space, and frequency domains have been verified by theoretical derivations and simulations.

ACKNOWLEDGMENT

REFERENCES

[1] S.Mumtaz, J. Jornet, J. Aulin, W. H. Gerstacker, X. Dong, and B. Ai, "Terahertz communication for vehicular networks," *IEEE Trans. Veh. Technol.*, vol. 66, no. 7, pp. 5617–5625, July 2017.

[2] H. Elayan, O. Amin, R. M. Shubair, and M. Alouini, "Terahertz communication: The opportunities of wireless technology beyond 5G," in *Proc. ICACT'18*, Marrakech, Morocco, Apr. 2018, pp. 1–5.

[3] X. Ge, K. Huang, C.-X. Wang, X. Hong, and X. Yang, "Capacity analysis of a multi-cell multi-antenna cooperative cellular network with co-channel interference," *IEEE Trans. Wireless Commun.*, vol. 10, no. 10, pp. 3298–3309, Oct. 2011.

[4] L. Xiang, X. Ge, C.-X. Wang, F. Y. Li, and F. Reichert, "Energy efficiency evaluation of cellular networks based on spatial distributions of traffic load and power consumption," *IEEE Trans. Wireless Commun.*, vol. 12, no. 3, pp. 961–973, Mar. 2013.

[5] J. M. Jornet and I. F. Akyildiz, "Channel modeling and capacity analysis for electromagnetic wireless nanonetworks in the terahertz band," *IEEE Trans. Wireless Commun.*, vol. 10, no. 10, pp. 3211–3221, Oct. 2011.

[6] G. A. Siles, J. M. Riera, and P. Garcia-del-Pino, "Atmospheric attenuation in wireless communication systems at millimeter and THz frequencies [wireless corner]," *IEEE Antennas Propag. Mag.*, vol. 57, no. 1, pp. 48–61, Feb. 2015.

[7] J. Sun, F. Hu, and S. Lucyszyn, "Predicting atmospheric attenuation under pristine conditions between 0.1 and 100 THz," *IEEE Access*, vol. 4, pp. 9377–9399, Nov. 2016.

[8] C. Jansen, R. Piesiewicz, D. Mittleman, T. Krner, and M. Koch, "The impact of reflections from stratified building materials on the wave propagation in future indoor terahertz communication systems," *IEEE Trans. Antennas Propag.*, vol. 56, no. 5, pp. 1413–1419, May 2008.

[9] R. Piesiewicz, C. Jansen, M. Koch, and T. Krner, "Measurements and modeling of multiple reflections effect in building materials for indoor communication systems at THz frequencies," in *Proc. GeMiC'08*, Hamburg-Harburg, Germany, Mar. 2008, pp. 1–4.

[10] S. Priebe, M. Kannicht, M. Jacob, and T. Krner, "Ultra broadband indoor channel measurements and calibrated ray tracing propagation modeling at THz frequencies," *J. Commun. Netw.*, vol. 15, no. 6, pp. 547–558, Dec. 2013.

[11] C. Jansen, S. Priebe, C. Moller, M. Jacob, H. Dierke, M. Koch, and T. Krner, "Diffuse scattering from rough surfaces in THz communication channels," *IEEE Trans. THz Sci. Technol.*, vol. 1, no. 2, pp. 462–472, Nov. 2011.

[12] F. Sheikh, D. Lessy, M. Alissa, and T. Kaiser, "A comparison study of non-specular diffuse scattering models at terahertz frequencies," in *Proc. IWMTS'18*, Duisburg, Germany, Jul. 2018, pp. 1–6.

[13] F. Sheikh, D. Lessy, and T. Kaiser, "A novel ray-tracing algorithm for non-specular diffuse scattered rays at terahertz frequencies," in *Proc. IWMTS'18*, Duisburg, Germany, Jul. 2018, pp. 1–6.

[14] S. Priebe, M. Jacob, C. Jansen, and T. Krner, "Non-specular scattering modeling for THz propagation simulations," in *Proc. EUCAP'11*, Rome, Italy, Apr. 2011, pp. 1–5.

[15] C. Han, A. O. Bicen, and I. F. Akyildiz, "Multi-ray channel modeling and wideband characterization for wireless communications in the terahertz band," *IEEE Trans. Wireless Commun.*, vol. 14, no. 5, pp. 2402–2412, May 2015.

[16] S. Priebe and T. Kurner, "Stochastic modeling of THz indoor radio channels," *IEEE Trans. Wireless Commun.*, vol. 12, no. 9, pp. 4445–4455, Sep. 2013.

[17] C.-X. Wang, J. Bian, J. Sun, W. Zhang, and M. Zhang, "A survey of 5G channel measurements and models," *IEEE Commun. Surveys Tuts.*, vol. 20, no. 4, pp. 3142–3168, 4th Quart., 2018.

[18] Y. Liu, C.-X. Wang, J. Huang, J. Sun, and W. Zhang, "Novel 3-D nonstationary mmwave massive MIMO channel models for 5G high-speed train wireless communications," *IEEE Trans.Veh.Technol.*, vol. 68, no. 3, pp. 2077–2086, Mar. 2019.

[19] S. Wu, C.-X. Wang, e. M. Aggoune, M. M. Alwakeel, and X. You, "A general 3-D non-stationary 5G wireless channel model," *IEEE Trans. Commun.*, vol. 66, no. 7, pp. 3065–3078, Jul. 2018.

[20] J. Huang, C.-X. Wang, R. Feng, J. Sun, W. Zhang, and Y. Yang, "Multi-frequency mmWave massive MIMO channel measurements and characterization for 5G wireless communication systems," *IEEE J. Sel. AreasCommun.*, vol. 35, no. 7, pp. 1591–1605, Jul. 2017.

[21] M. Ptzold, *Mobile Radio Channels*, 2nd ed. West Sussex, U.K.: Wiley, 2012.

[22] R. He, O. Renaudin, V. Kolmonen, K. Haneda, Z. Zhong, B. Ai, and C. Oestges, "Characterization of quasi-stationarity regions for vehicle-to-vehicle radio channels," *IEEE Trans. Antennas Propag.*, vol. 63, no. 5, pp. 2237–2251, May 2015.